Analysis of Gibbsian Segregation at Heterophase Cu-MnO Interfaces

Mogck, Stefan; Kooi, Bart J.; Hosson, Jeff T. De

Published in:
Interface Science

DOI:
10.1023/B:INTS.0000012293.11631.48

Publication date:
2004

INTERFACE SCIENCE 12, 39–56, 2004

Analysis of Gibbsian Segregation at Heterophase Cu-MnO Interfaces

STEFAN MOGCK, BART J. KOOI AND JEFF T. DE HOSSON*
Department of Applied Physics, Materials Science Center and the Netherlands Institute for Metals Research, University of Groningen, Nijenborgh 4, 9747 AG Groningen, The Netherlands
s.mogck@phys.rug.nl
j.b.kooi@phys.rug.nl
hossonj@phys.rug.nl

Abstract. An alternative methodology to analyze Gibbsian segregation at heterophase interfaces with transmission electron microscopy (TEM) is presented and discussed. In this approach the actual concentration of the segregating element in a monolayer at the interface is obtained. This is in contrast to line scans or maps where the concentrations determined are a convolution of the concentration profiles with the electron probe and where for general interfaces the deconvolution problem can not be solved accurately. This is possible because the present approach uses explicitly the information offered by hetero-interfaces. The method is tested on the possible segregation of indium and gallium dissolved in a Cu matrix to interfaces between MnO precipitates and the Cu matrix. The occurrence of indium segregation is clearly demonstrated and the In concentration in the terminating Cu monolayer at the parallel $\{111\}$ Cu/MnO interface is determined to be 15 ± 3 at.%, whereas the average In concentration in the Cu matrix is 3.8 ± 0.4 at.%. Further it was found that indium effectively blocks gallium segregation towards the oxide side of the interface. On the other hand, the presence of gallium does not influence the segregation of indium. Explanation for the gallium segregation at the oxide side relies on a thin spinel type $Ga_xMn_yO_4$, which reduces the misfit at the metal-oxide interface.

Keywords: segregation, interface, Cu-MnO, transmission electron microscopy, X-ray energy dispersive spectrometry

1. Introduction

In multi-component systems alloying elements or impurities often segregate to homo- or hetero-phase interfaces. Segregation may influence many material properties, for instance mechanical, electrical, magnetic and chemical properties [1]. Indeed, segregation to interfaces in polycrystalline materials may have both beneficial and detrimental effects on the materials performance. The importance of segregation to interfaces is determined primarily by the inherent inhomogeneity of interfaces, i.e. the fact that physical and chemical properties may change dramatically at or near the interface itself. The accumulation of impurity atoms at grain boundaries and surfaces leads to the formation of a very narrow zone, of the order of a few lattice spacings, with different chemical composition. As a result of sharp concentration gradients an isotropic bulk solid may change locally into a highly anisotropic medium. Very small bulk concentrations of impurity atoms can lead to significant amounts of those atoms at the grain boundary. This can drastically change the response of a material on loading and can eventually lead to brittle failure of an otherwise ductile material. Although embrittlement by impurity segregation is frequently observed, segregation can also have a ductilizing effect on brittle materials, depending on both impurity and matrix elements.

In contrast to surface or grain boundary segregation, hetero-phase boundary segregation has received very little attention [2, 3] because of the experimental difficulties to demonstrate the presence of small amounts

*To whom all correspondence should be addressed.

of a solute material at interfacial planes. Commonly used techniques to study segregation such as Auger microscopy cannot be used, because it is often very unlikely that the material will break at the interface. Only recently, techniques such as analytical (S)TEM (employing X-ray energy dispersive spectrometry or parallel electron energy loss spectroscopy), atom probe field ion microscopy (both 1-D and 3-D) and Z-contrast in STEM have become sufficiently developed to allow study of segregation down to a single monolayer at a hetero-interfaces [4–7].

Nowadays three methods are available to reveal segregation at interfaces using analytical (S)TEM at edge-on oriented interfaces in a TEM foil: (i) taking a line scan, (ii) chemical mapping, (iii) using a scan raster. A standard method to reveal segregation at interfaces using analytical TEM is to perform line-scans across an interface edge-on oriented in the TEM foil. In this way segregation of antimony towards the $\{111\}$ Cu/MnO interface was demonstrated [7]. A drawback of line scans and maps is related to drift of the sample and/or the electron beam. The sample drift may occur due to local heating by the electron beam and cannot be fully eliminated. Both kinds of drift are harmful for a detailed analysis, because in order to detect small enrichments in just one monolayer the steps between measurement points have to be made small, and the detection time per point has to be made sufficiently large to record significant signals. A line scan is in general statistically inadequate to analyze strong concentration gradients at interfaces, due to the lack of a sufficient number of spots in the crucial region. In (S)TEM mode the concentrations measured are not the actual ones, but convoluted spatially with the electron probe. In the case where the size of the fluctuations in concentration is smaller than the probe size (for instance an enrichment in only 1 monolayer with a thickness of 0.2 nm whereas the effective probe size is for instance 1 nm) the measured concentration depends sensitively on the *exact* position of the electron probe with respect to the concentration fluctuation. Using a line-scan or elemental mapping the position of the probe is in general not known accurately enough to obtain the actual concentrations, that is to say to perform the deconvolution. A scan raster overcomes these problems of drift and inadequacy, but at the expense of a decrease in detection sensitivity due to averaging over a larger volume.

Another way to circumvent this problem without losing detection sensitivity is offered by a different approach. The basic idea is that the measured solute concentration is plotted against one of the two measured solvent concentrations showing an abrupt concentration change at the interface and fitted with theoretical curves based on assumed concentration profiles that are convoluted with a (Gaussian) function mimicking the electron probe. It should be stressed, however, that this methodology is specifically applicable to *heterophase* interfaces. This approach to measure segregation towards heterophase interfaces using analytical TEM avoids the need of a dedicated STEM or STEM attachment (although our approach can be improved when combined with STEM) and which also avoids the problems associated with line-scans. The method can be applied to any system, in which abrupt and sufficiently large differences in concentrations of the solvents on both sides of the interface are present. This requirement is mostly met by hetero-interfaces. Compared to approaches that can be applied to all boundary types this requirement is a limitation, but on the other hand the present methodology uses explicitly the special properties of hetero-interfaces. This makes the present approach either more detection sensitive or less vulnerable to drift or quantitatively more accurate than methods that are also applicable to homo-interfaces. More details on the comparison of the present methodology with other approaches are given at the end of the discussion (Section 4.3). In the next section the method is introduced, which aims at predicting the solute-solvent plots for different experimental parameters. The methodology is illustrated to determine the amount of segregation of solute atoms at various metal-ceramic interfaces, which are formed after internal oxidation of a Cu-1 at.%Mn alloy. Finally, the Analtical TEM results are also combined with results from High-Resolution TEM in order to verify if the segregation causes observable deviations in the atomic structure of the interface.

2. Model

To be able to quantify the amount of segregation at a hetero-interface A(B)/C(B), it is necessary to correlate the measured concentration in some way to the *exact* position of the probe with regard to the interface. A and C are the solvents on both sides of the interface and B is the solute. In principle it is always possible to know the position of the probe with respect to the interface if abrupt and sufficient large differences in concentration of the solvents A or C occur at the interface. For instance A has a negligible solubility in

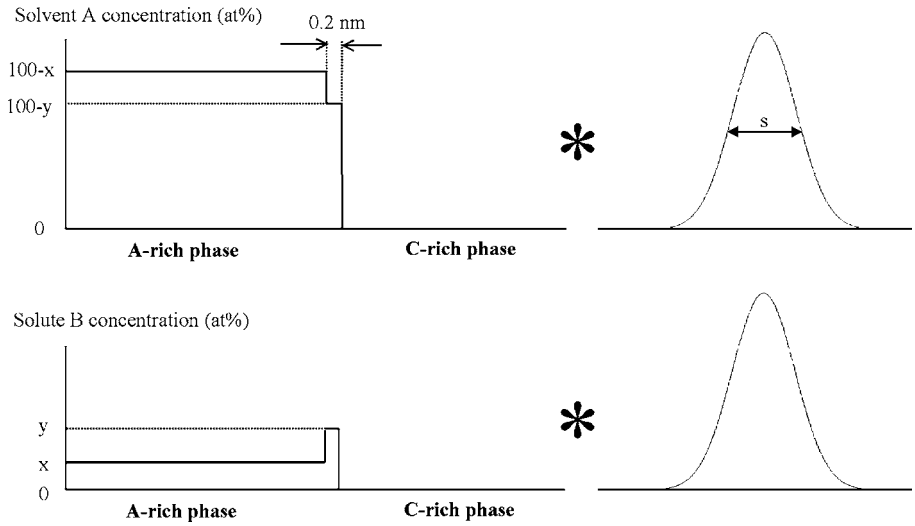

Figure 1. Assumed concentration profiles for the solvent A and solute B at an A(B)/C(B) heterophase interface and indication of the electron probe with which these concentration profiles are measured (convoluted).

C, but C may be dissolvable in A. Instead of making a line-scan with a small probe across the interface, a large number of measurements are made directly on top of the edge-on interface, together with a limited number of measurements on the surrounding area, both on the A- and C-rich sides of the interface. This is possible manually using a nano-probe in a TEM without a scan raster or automatically by using a STEM (attachment). The relative concentration of solute B can be related to the solvent concentration A. If the concentration A is maximum the probe is on the A-rich side and if the concentration of A is minimum it is on the C-rich side. Half way between this maximum and minimum it is exactly symmetrically positioned on top of the interface. If there is no solute enrichment at the interface, the solute concentration B plotted versus the solvent concentration A results in a straight line. If the measurements on the boundary lie above the straight line, the solute segregates towards the boundary. If they lie below the line, the solute is depleted at the boundary. Note the key point that a plot of solute versus solvent is made and not a standard one where the solute is plotted spatially (either in a line scan, X-Ray map or an energy-filtered image). In this way the horizontal axis is stretched such that the end points correspond to the positions where the nano-probe starts to touch the interface and maximum sensitivity occurs where the concentration gradients are largest.

The next central step of the approach is that the experimentally plotted data of solute B versus solvent A are modeled and fitted. As an example the most likely case is modeled, i.e. with concentration profiles near the boundary as depicted in Fig. 1. The solute concentration B inside the solvent C is set equal to zero, and inside solvent A equal to x at.%. The segregation is assumed to be limited to just one monolayer (ML), with a width of 0.2 nm. In this ML there are only solvent A and solute B atoms present. The concentration of the solute in the ML amounts to y at.%. To model the results from Analytical TEM measurements, these concentration profiles are convoluted with a Gaussian function. This function represents the electron probe, which has in perfect conditions (i.e. perfect electron source and a perfect alignment of the microscope column) a Gaussian intensity distribution and where the probe size includes beam broadening in the sample. For the convolution fast Fourier transformations of the concentration profiles and of the electron probe are performed, multiplied and subsequently Fourier transformed again. Actually, three parameters are free to choose. These are the solute B concentration in solvent A (x), the solute B concentration in the ML at the interface (y) and the full width half maximum (FWHM) probe size (s). The latter depends on the accelerating voltage, the initial probe size and the thickness and density of the TEM specimen locally. As a parameter to describe our Gaussian function we use FWHM, but the Gaussian and the results remain of course identical if we would have based it on for instance full width tenth maximum which is also often used to define the probe size.

The model seems to have a one-dimensional character (cf. Fig. 1). However, extending it to 2-D, i.e. with a planar interface and a rotationally symmetric Gaussian probe, yields identical results due to the special properties of a Gaussian function. The idea is to use this description by varying the value of y. The best fit yields the solute concentration in the ML at the interface. Figure 2(a) shows the model results for varying solute concentrations in the ML. In the model x is set to 3.5 at.%, y is varied between 3.5 and 50 at.% and s is taken as 1.4 nm. This seems a reasonable assumption

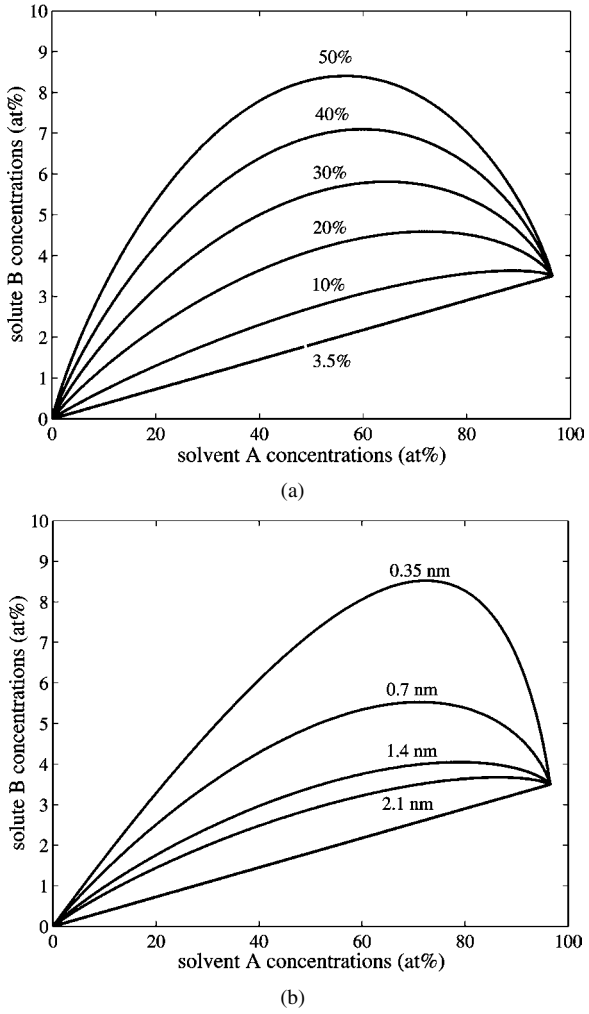

Figure 2. (a) Model results for various solute B concentrations y in the terminating monolayer of the solvent A at the hetero-interface. The solute B concentration x in the bulk of solvent A is 3.5 at.%. The probe size s is 1.4 nm. (b) Model results for various probe sizes s. The solute B concentration y in the terminating monolayer of the solvent A at the hetero-interface is set to 15 at.%. The solute B concentration x in the bulk of solvent A is 3.5 at.%.

for a 200 kV beam, an initial probe size of 0.7 nm and a thickness of Cu of 30 nm [8]. As can be expected, the probe size has a large influence on the resulting graphs. Using a smaller probe size, the influence of the enriched monolayer on the total solute concentration will increase and as a result the deviation from the straight line will be more pronounced. This is shown in Fig. 2(b), in which the results are shown for varying probe sizes. To achieve these results x is set to 3.5 at.%, y to 15 at.% and s varies between 0.35 and 2.1 nm.

To extend the potential possibilities of the model a bit further the simple concentration profiles assumed in Fig. 1 are slightly adapted. Suppose that segregation does not occur at a single ML, but at a double layer at the interface. This double layer can be the last two terminating layers of solvent A (indicated as AA) or can be the terminating layer in each of the solvents A and C (indicated as AC). Figure 3(a) and (b) show the results if the concentration solute B in both layers is 15 at.% and reproduces the result for 30 at.% B in the single terminating layer in solute A (indicated as A) for a FWHM of the electron probe of 1 and 2 nm, respectively. The solute concentration in the bulk of A is 3.5 at.% and in the bulk of C is negligible. Figure 3 shows that in principle it is possible to distinguish between these different types of segregation on the basis of the different shapes of the curves. However, taking the experimental accuracy of the relative concentration determination into account (not the absolute one which is worse) it will be hardly possible to make this distinction in practice. However, the smaller the probe size the larger the possibility that this distinction can be made. In case of Gibbsian segregation it is often assumed that the enrichment occurs in a single ML at the interface [9–11]. For instance the well-known McLean isotherms rely explicitly on this assumption [11].

3. Experimental

An alloy containing copper with 1 at.% manganese was made in a high-frequency furnace by melting the pure constituents (99.99% by weight) in an alumina crucible under oxygen-free argon protective atmosphere. Ingots were homogenized (1 week at 700°C in an evacuated quartz tube) and subsequently cold rolled from 4 mm down to 0.5 mm. The interfaces between manganese oxide and copper were obtained by internal oxidation using the Rhines Pack technique [12] (an envelope of Cu-foil is filled with the sample and Cu, Cu_2O and Al_2O_3 powder in a volume ratio of about 1:1:1

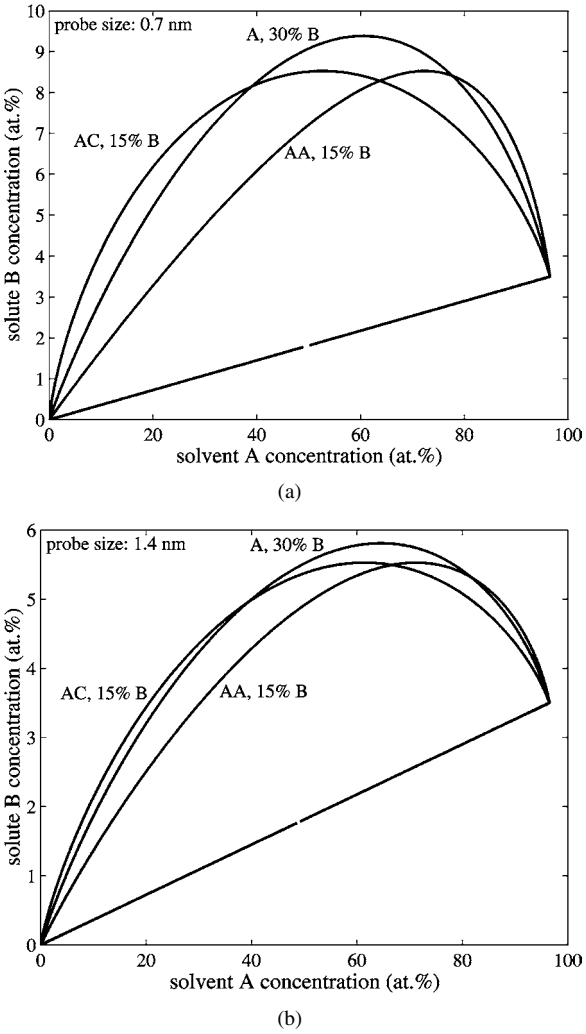

Figure 3. Model results for solute B concentrations of 30 at.% in the terminating monolayer of the solvent A (indicated as A), of 15 at.% in the last two MLs of solvent A at the interface (indicated as AA) and of 15 at.% in the last ML of solvent A and the first ML of solvent C at the interface (indicated as AC) for probe sizes s of (a) 0.7 nm and (b) 1.4 nm.

and placed in an evacuated quartz tube for 17 hours at 900°C). Approximately 5 at.% indium was introduced by means of a vapor treatment. The indium was placed together with the sample, without making direct mutual contact, inside an evacuated quartz tube for 5 days at 800°C.

The resulting In-free system is extensively described in references [13–15]. In the copper matrix MnO precipitates with a cube-on-cube orientation relation with the matrix develop having a truncated octahedral shape. The MnO has a NaCl-type crystal structure and the average size of the particles is 200 nm. A large mismatch of 22.9% is present between all atomic spacings of Cu and MnO, which leads to the formation of semi-coherent interfaces. Two types of interfaces are formed. At the $\{111\}$ octahedral interfaces a trigonal network of edge dislocations, with line direction $\langle 110\rangle$ and Burgers vector $1/6\langle 112\rangle$, is present. At the $\{100\}$ truncation interfaces only one of the two fcc-sublattices in the MnO is continued into the copper. TEM samples were prepared by grinding, dimpling and ion milling 3 mm discs to electron transparency.

A second example of segregation to heterophase interfaces concerns Ga. After internal oxidation approximately 3.5 at.% gallium was placed together with the sample, without making mutual contact, inside an evacuated quartz tube for 1 week at 700°C. After 1 week nearly all gallium is dissolved more or less homogeneously in the copper matrix. Next, two different treatments were used. One consisted of introducing approximately 3.5 at.% indium in the copper matrix using the same treatment as for gallium during 1 week at 750°C. The other consisted of the same annealing treatment but without indium present.

The XEDS measurements were performed using a JEOL 2010F, field emission gun TEM operating at 200 kV equipped with an EDAX XED-spectrometer with a super ultra thin window. A double-tilt beryllium sample holder was used. Before the measurements, the sample was tilted to make the incoming electron beam parallel to a $\langle 110\rangle$ Cu matrix orientation. This ensures that all the planar interfaces are edge-on. The measurements were performed using the two smallest possible probes, with diameters of 0.5 and 0.7 nm FWHM. In XEDS measurements the sample was always tilted towards the detector over an angle between 10 and 30 degrees. The dead time was never larger than 40% and never smaller than 10%. This was achieved by choosing time constants varying inbetween 100 and 35 μs, corresponding to an energy resolution relative to MnKα varying from 135 to 145 eV, respectively. After a manual background subtraction, quantification of XED-spectra was performed using the Cliff-Lorimer ratio technique in the thin-film approximation [16]:

$$\frac{C_A}{C_B} = k_{AB}\frac{I_A}{I_B} \tag{1}$$

where C_A and C_B are the concentrations of element A and B in the specimen, I_A and I_B are the measured intensities in the X-ray spectrum and k_{AB} is the

Cliff-Lorimer factor. In the present research the theoretical k_{AB} factors due to Zaluzec [17] were used. A large number of spectra were obtained by positioning the electron beam on the interface, measuring for 35 seconds and subsequently shifting the beam to another part of the interface. These measurements were accompanied by a small number of spectra from the areas on both sides of the interface. After quantification the indium concentration was related to the copper concentration and compared with the model description.

For HRTEM a JEOL 4000 EX/II, operating at 400 kV (spherical aberration coefficient: 0.97 ± 0.02 mm, defocus spread: 7.8 ± 1.4 nm, beam semi-convergence angle: 0.8 mrad) was used. HRTEM images were obtained by digitizing negatives using a CCD camera and the gray scale was adapted to achieve reasonable brightness/contrast. HRTEM images were not filtered.

4. Results and Discussion

4.1. XEDS

XEDS measurements taken on the copper matrix and on MnO precipitates indicated a composition as depicted in Table 1. The errors indicated represent $\pm 2\sigma$ based on Gaussian statistics. This means that the chance is 95% that the value found for the concentration will be within the true value for the concentration, if there would be no other sources of error such as possible systematic errors introduced by the k_{AB} factors. The small amounts of Mn and O found in the Cu matrix and the small amounts of Cu found during the measurement on the MnO precipitate are attributed to spurious X-rays, since all these measurements were taken close to the interface. From these measurements it becomes clear that no indium is present in the precipitates.

To demonstrate segregation to an interface with the segregating element present at one side of the interface, it is necessary to correlate the measured concentration to the position of the probe with respect to the interface. This can be done using the method described in Section 2. Various measurements were performed on the interface, together with a limited number of measurements on the surrounding area, both in the matrix and in the precipitate. The measured relative indium concentration can then be related to the copper concentration. If there is no indium enrichment at the interface, the only source of indium counts is from the indium in the bulk. Consequently, independent of the position of the probe, the indium concentration divided by the copper concentration will always be a constant. Plotting the indium concentration against the copper concentration will result in a straight line. If the points resulting from the measurements on the boundary lie above the straight line, which is determined by the measurements in the bulk and the precipitate, the indium segregates towards the boundary. If they lie below the line, the indium is depleted at the boundary (see Section 2). Figure 4 shows the result of a measurement performed on a parallel $\{111\}$ Cu/MnO interface [18].

This measurement was made using an 0.7 nm FWHM electron probe. This probe is chosen instead of the smaller 0.5 nm probe, because the latter yields fewer counts when an interface close to the hole in the TEM specimen is studied. If the 0.5 nm probe is used, an interface has to be found in a thicker region of the specimen. The beam broadening inside a specimen goes with the thickness to the power 3/2 [19]. Therefore, no real improvement is achieved upon using the smaller beam. The best interfaces are found close to the hole in the TEM specimen. In these thin regions the change of completely or partially coverage of the small precipitate by the copper matrix is the smallest.

Table 1. XEDS results for the Cu matrix and MnO precipitates (average of 5 spectra).

	Cu (at.%)	Mn (at.%)	O (at.%)	In (at.%)
Copper bulk	92.6 ± 1	1.1 ± 0.5	2.5 ± 1	3.8 ± 0.4
MnO precipitate	2.8 ± 0.6	50.1 ± 1	46.9 ± 1	0.1 ± 0.1

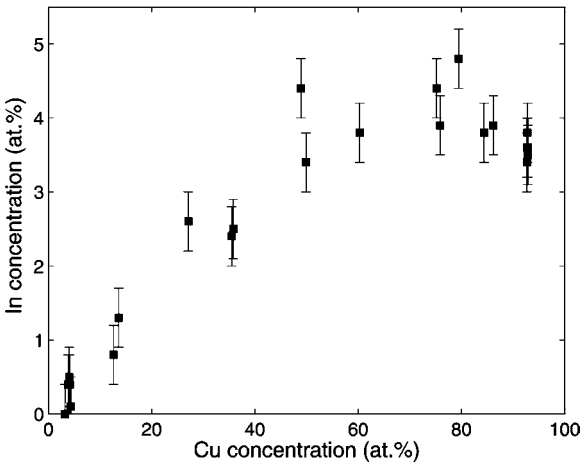

Figure 4. XEDS results obtained for a parallel $\{111\}$ Cu/MnO interface. The measurement was performed with an 0.7 nm FWHM probe.

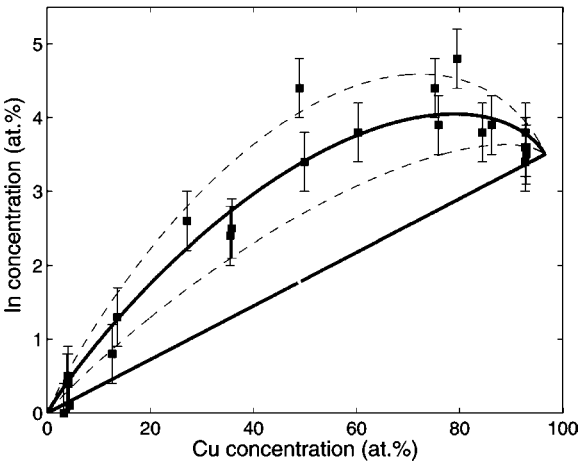

Figure 5. XEDS results (cf. Fig. 4) together with model curves. The curves hold for an indium concentration in the Cu matrix of 3.5 at.% and a probe size of 1.4 nm. The central solid curve holds for an In concentration of 15 at.% in the terminating monolayer of the Cu at the Cu/MnO interface and the lower and upper dashed curves correspond to 10 and 20 at.%, respectively.

If a line is drawn from the center of the first cluster of points (measurements in the MnO) to the last few points (bulk), it is clear that all other point lie above this line (Fig. 4). This unambiguously indicates a segregation of indium towards the Cu/MnO interface.

In Fig. 5 the XEDS measurements from Fig. 4 are combined with the model, where the solid curve holds for x: 3.5 at.%, y: 15 at.% and s: 1.4 nm. The curve for these values is assumed to be the best fit. It is clear from the dashed curves that varying y to either 10 or 20 at.% resulted in a poorer fit. The curve fits the data points rather well, with the exception of two points, which have a higher indium concentration than predicted. This is possibly caused by a non-homogeneous indium concentration along the boundary. The start and end points are also not fitted very accurately and it is caused by the appearance of spurious X-rays. The model assumes no copper and indium in the MnO precipitate and therefore all the curves go through the origin. The measurements performed on the MnO reveal a clear copper signal and also a very small fraction of indium. At the end points, the same problem arises. Since the model assumes 3.5 at.% indium in the matrix, all the curves end in the point (96.5, 3.5). The measurements on the bulk however, show a total of 3.6 ± 1 at.% manganese and oxygen, which is again caused by spurious X-rays. Out of the six interfaces analyzed, four showed very similar results as the one shown in Fig. 4 and for two interfaces a weaker effect was observed, although in all cases the occurrence of segregation was obvious.

4.2. HRTEM

A HRTEM image of a Cu(In)/MnO interface is shown in Fig. 6. The interface is constituted by parallel $\{111\}$ planes of Cu and MnO and viewed along their common $\langle 110 \rangle$ directions. The interface is positioned in an edge-on orientation. The dots on the upper half of the picture correspond to columns of manganese atoms (the oxygen atoms are not visible under the present imaging conditions; according to the image simulations below). The dots on the lower half correspond to columns of Cu-atoms. Just like in the high-resolution image of a clean (In-free) Cu/MnO interface, the mismatch is relieved by a trigonal network of edge-type misfit dislocations with line direction $\langle 110 \rangle$ and Burgers vector $1/6\langle 112 \rangle$ [15]. We extensively studied misfit-dislocation networks at Cu/MnO and Cu/MgO interfaces by comparing experimental HRTEM images with simulated images based on atomistic calculations yielding relaxed atomic structures of the interfaces [20]. In Fig. 6 one array of misfit dislocations, with a repeat distance of five or six atomic planes in the copper, is observed end-on. The cores of these dislocations are situated at the centers of the darker areas periodically present at the interface shown in Fig. 6. Two other dislocation arrays are inclined $\pm 60^\circ$ with respect to the viewing direction. Comparing Fig. 6 with HRTEM images of clean Cu/MnO $\{111\}$ interfaces indicates that the dark areas at the position of the cores of the edge-on dislocation are clearly more pronounced in Fig. 6.

Figure 7 shows the results of atomistic calculations for the parallel $\{111\}$ Cu/MnO interface. The mismatch used in the simulations can be taken close to the real mismatch under the restriction that commensurate blocks of atoms are taken for the metal and the oxide. The mismatch for Cu/MnO is approximated by 16 periods in the Cu versus 13 periods in the "oxide", i.e. 23.1% mismatch which is very close to the real 22.9% mismatch. The relaxed structure (only the metal side is relaxed, the oxide is assumed to be rigid) is shown for the terminating oxygen and metal $\{111\}$ planes at the interface are viewed along the interface normal. The small spots represent the last oxygen-layer in the MnO and the larger circles the first copper layer. The gray-scale of the Cu atoms in Fig. 7 indicates the distance from the Cu atoms to the planar interface (parallel to the planar O$\{111\}$ plane); white indicates the

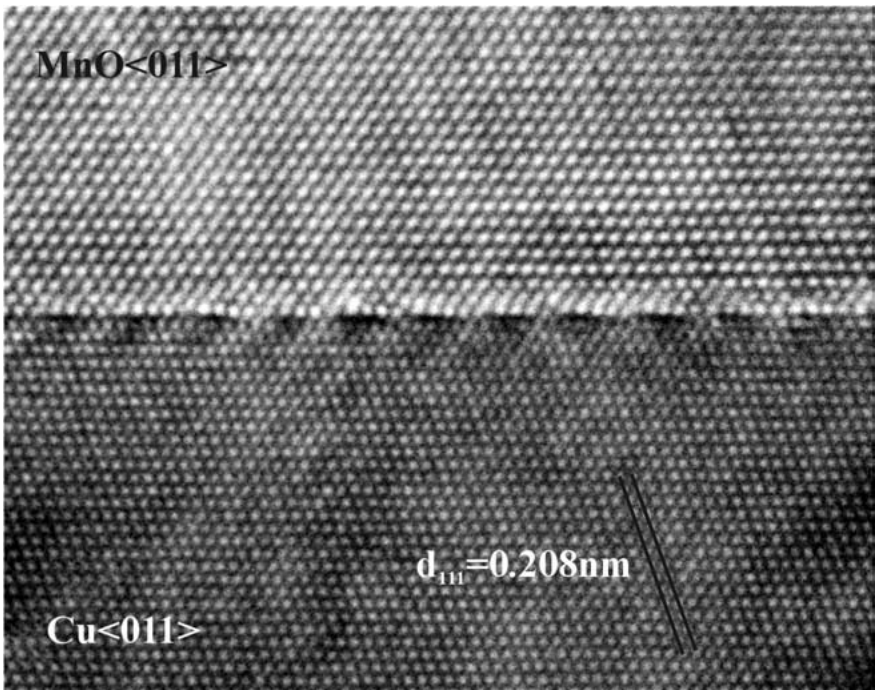

Figure 6. HRTEM image of a parallel {111} Cu/MnO interface as viewed along a common ⟨110⟩ of Cu and MnO. Intensity modulations can be observed with an edge-on array of misfit dislocations at the centers of dark areas periodically present along the interface.

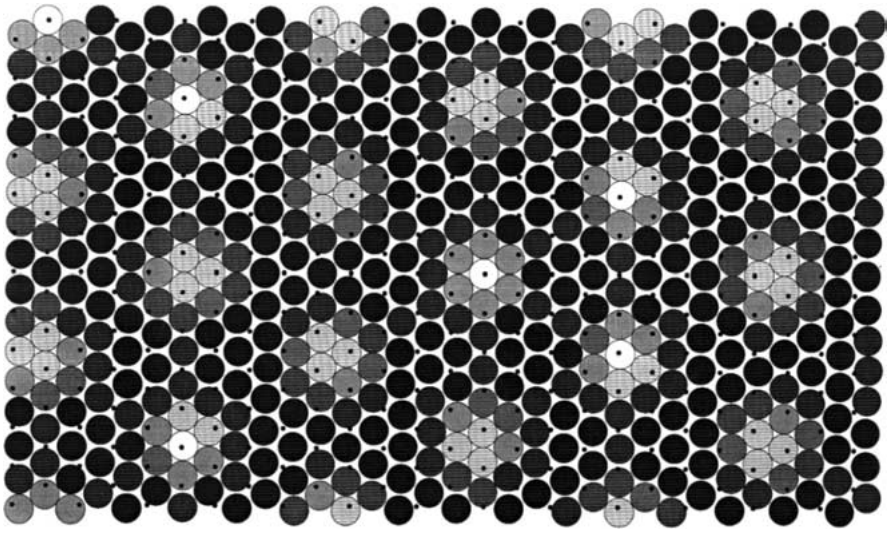

Figure 7. Relaxed structure (results of atomistic calculations) for the parallel {111} Cu/MnO interface with a mismatch of 23.1% (16 periods in the metal versus 13 in the oxide). The terminating Cu and oxygen {111} planes at the interface are shown as viewed along the interface normal ⟨111⟩. Small black dots denote the oxygen atoms in the terminating layer of the oxide and larger circles with different gray levels denote the Cu atoms; the darker the indication of the Cu atoms the smaller the distance between the Cu atoms and the planar interface.

largest and black the shortest distance. In terms of discrete dislocations the simulations indicate that a trigonal network of misfit dislocations with line direction ⟨110⟩ and Burgers vector 1/6⟨112⟩ is present. At the centers of the triangles formed by the dislocation lines, the Cu atoms are in hollow 3-fold coordinated with O atoms and are attracted to the interface. In principle there are two types of triangles if we are concerned

with the stacking sequence perpendicular to the interface. In one triangle-type the layers are correctly fcc stacked, whereas for the other triangle a stacking fault (local hcp stacking) occurs at the interface. The O-nodes according to Bollman's O-lattice theory [21] occur only at the centers of the correctly stacked triangles. However, according to the atomistic calculations generalized O-nodes can be defined which occur at the interface at the centers of both triangle-types. At the positions of the dislocation nodes, i.e. the intersection points of the dislocation lines with the 3 different ⟨110⟩-type directions, the copper atoms are on top of the O atoms and are pushed away from the interface. These results of Cu atoms being attracted and pushed away from the interface are consistent with the periodic wave-like separation observed at the interface in the experimental HRTEM image (Fig. 6). The calculations however were performed for a clean Cu/MnO system. In HRTEM images these intensity modulations along the interface could only be observed with great difficulty. In contrast the intensity modulations are easily observable in the In-segregated Cu/MnO interfaces (cf. Fig. 6). Obviously the presence of indium at the interface intensifies the wavelike seperation between the terminating matrix and oxide planes at the interface. Indium atoms are rather big; the atomic radius of indium is 167 pm compared to 128 pm for copper. The copper atoms in the center of the triangles formed by the dislocation lines, experience a tensile stress. Therefore, at these positions it is very favourable for copper interfacial atoms to exchange with the bigger indium atoms in the bulk. Hence a driving force for segregation of indium from the matrix to the interface is present. The net result is however, that the compressive stresses on the remaining Cu atoms at the dislocation cores increase even more, thereby increasing the wavelike separation effect in accordance with the experimental HRTEM observations.

Figure 8 gives the results of image simulations (MacTempas), where the relaxed 3-dimensional block of atoms obtained by the atomistic calculations was used as input structure. A proper resemblance between simulated and experimental HRTEM image is obtained for a defocus of −60 nm and a thickness of 5 nm (cf. Fig. 8(a)). The image simulation indicates that a dark intensity modulation is present along the interface, although it is not easily recognizable in Fig. 8(a). In Fig. 8(b) results of image simulations for zero defocus (and 5 nm thickness) are shown and under these imaging conditions the intensity modulations along the interface are pronounced. In the case of a non-relaxed structure, i.e. incoherent Cu/MnO {111} interface, such intensity modulations are absent. The intensity modulations of Fig. 8 compare reasonably with the experimental observed one, but appears less pronounced, particularly bcause it should be more easily detectable in a noise-free simulated image. However, the fact that it is less pronounced is not remarkable, because the

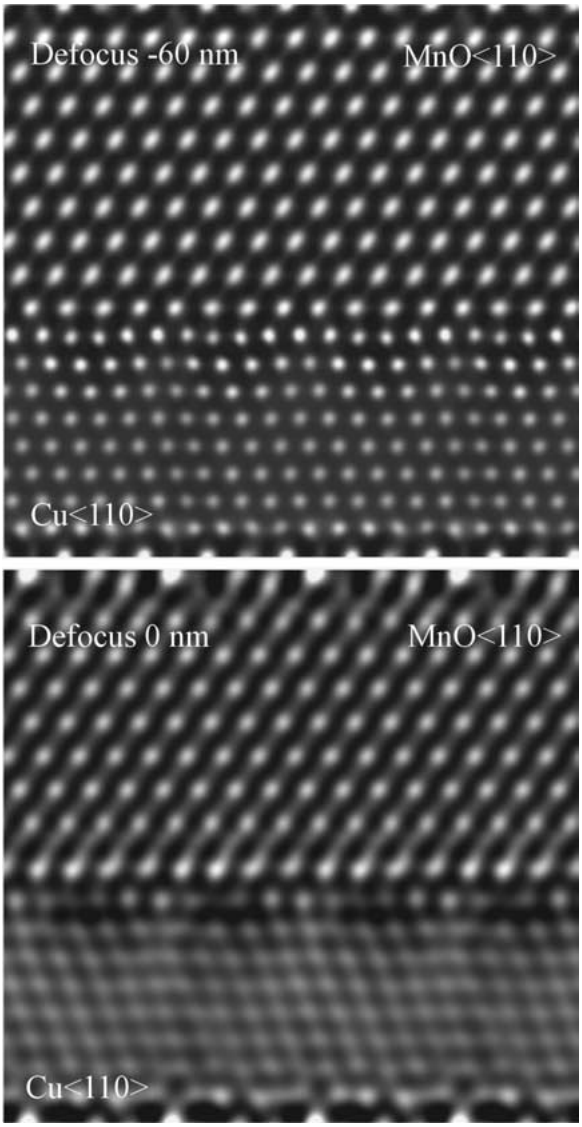

Figure 8. Image simulations (MacTempas) of the parallel {111} Cu/MnO interface for a thickness of 5 nm and a defocus of −60 nm (top) and 0 nm (bottom). A relaxed structure (results of atomistic calculations) of the interface with a mismatch of 25% (5 periods in the metal versus 4 in the oxide), giving similar results as the one shown in Fig. 7, was used as input structure for the simulation.

simulated image holds for the clean Cu/MnO interface. As already explained above the presence of indium at the interface intensifies the wavelike seperation between the terminating matrix and oxide planes at the interface and thus makes the intensity modulation more pronounced. Furthermore, the image simulation shows that at the positions of the dislocation cores, where the columns of copper atoms are less neatly stacked (cf. Fig. 7), a decrease in intensity of the bright dots in the HRTEM image occurs. Also this result is in accordance with the experimental observation (cf. Fig. 6).

Based on Fig. 7 a reliable estimate for the favourable indium concentration in the terminating metal monolayer (ML) at the Cu/MnO $\{111\}$interface can be made. If in all centres of the triangles formed by the dislocation lines (i.e. at the generalized O nodes) 1 to 3 copper atoms (i.e. 2 on average) are replaced by indium, a total of 72 In atoms will be present in the ML at the interface for the cell depicted in Fig. 7. Since a total of 522 positions are available in the ML of this cell, the indium content would be $14 \pm 7\%$. This is remarkably close to the experimentally obtained concentration of $15 \pm 3\%$ for indium in the ML. So, the conclusion of the analysis in this section is that In atoms segregate to the parallel $\{111\}$ Cu/MnO interface such that they substitute Cu atoms near the generalized O-node positions in the trigonal network of misfit dislocations. Because the number of favourable positions around each O-node will logically vary in-between 1 to 3 an accurate estimate for the expected indium concentration in the ML at the interface can be given.

As a second illustration of the methodology we concentrate now on the Ga segregation. Figure 9 shows the gallium concentration across a $\{111\}$ Cu-MnO interface just after the introduction of gallium into the internally oxidized Cu 1 at.% Mn. There is hardly any segregation of gallium recognizable. Thus, all the measured gallium concentrations versus the copper concentration across the interface can be described with a straight line. The fitting procedure assuming an effective probe size (FWHM) of 1.4 nm already indicates a gallium concentration of 1.8 at.% per monolayer in the first two monolayers of the oxide. The reason why we assume that the gallium is in the first two monolayers of the oxide will be discussed later. Note that the gallium concentration in the copper matrix is 3.8 ± 0.4 at.% (homogeneous). After 1 week at 750°C for the intake of indium, segregation of gallium is rather limited but already unambiguously detected. Only a small concentration of 2.5 at.% per monolayer is present in the first

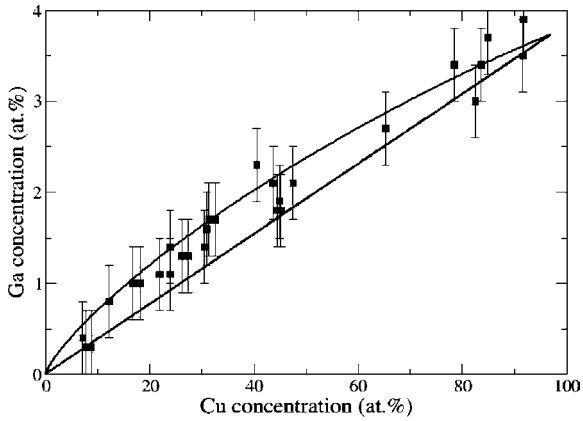

Figure 9. After Ga dissolution at 700°C for 1 week into internally oxidized Cu 1 at.% Mn, about 3.8 at.% Ga is dissolved in the copper matrix. The almost straight line indicates that Ga does not significantly segregates at the interface.

two monolayers of the oxide side of the interface (see Fig. 10). Already at this stage the fitting procedure clearly indicates that the data are better fitted with a concentration profile that assumes the gallium to be in the first monolayer or the first two monolayers of the oxide instead of the outermost monolayer of the metal matrix. Note that now the gallium concentration in the copper matrix has dropped to 1.9 ± 0.3 at.%. Thus, it appears that during the heat treatment and the dissolution of indium the gallium concentration at the interface obtains more or less the value that was originally present in the copper matrix. In the copper matrix

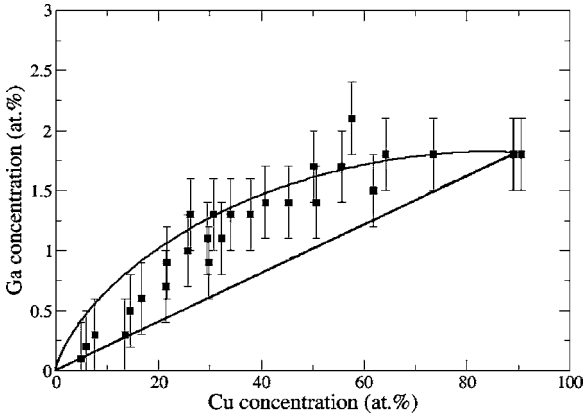

Figure 10. XEDS results together with the model curve. The curve holds for a Ga concentration in the copper matrix of 2 at.% and a probe size of 1.4 nm. The best match of the model curve with the XEDS measurement is reached with a Ga concentration of 2.5 at.% in the first two MnO monolayers at the Cu-MnO interface.

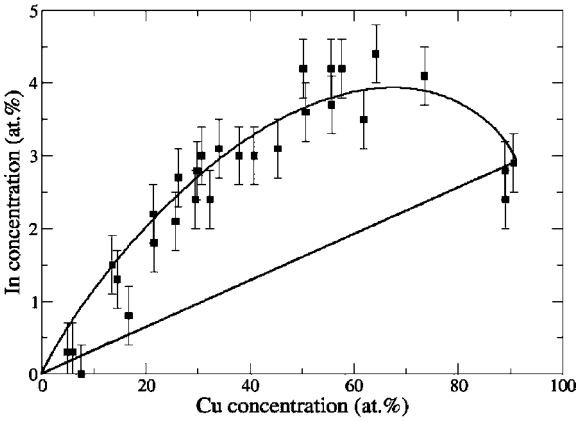

Figure 11. XEDS results together with the model curve. The curve holds for an In concentration in the copper matrix of 3.0 at.% and a probe size of 1.4 nm. The best match of the model curve with the XEDS measurement is reached with an In concentration of 17.6 at.% in the outermost copper monolayer at the Cu-MnO interface.

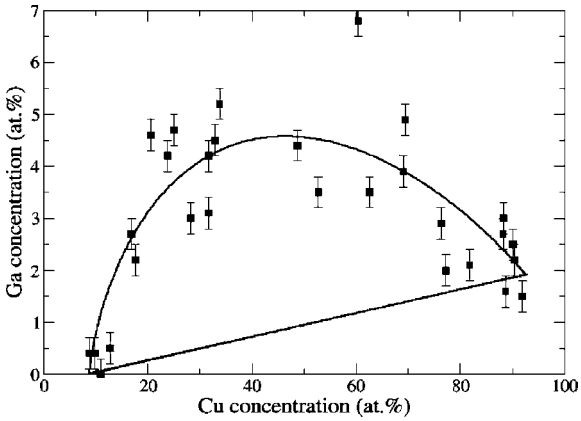

Figure 12. XEDS results together with the model curve. The curve holds for a Ga concentration in the copper matrix of 2.0 at.% and a probe size of 1.4 nm. The best match of the model curve with the XEDS measurement is reached with a Ga concentration of 14.3 at.% in the first two monolayers at the oxide side of the Cu-MnO interface.

itself the concentration of gallium decreases due to the segregation of gallium at grain boundaries and due to the formation of spinel-type $Ga_xMn_yO_4$ precipitates.

After the dissolution of indium, the segregation of indium occurs at the Cu/MnO interfaces as shown in Fig. 11. The presence of indium and gallium in Cu 1 at.% Mn results in an indium segregation of approximately 17 at.% in the terminating copper monolayer at the parallel $\{111\}$ Cu/MnO interface, whereas the average indium concentration in the copper matrix was only 2.9 at.% (see Fig. 11). Indium segregation of 17.6 at.% in the terminating monolayer is very similar to previous measurements of indium segregation of 15 at.% without the presence of gallium at the Cu-MnO interface. Apparently, there is no influence of the presence of gallium on the indium segregation to $\{111\}$ Cu-MnO interfaces.

In order to investigate the influence of gallium segregation without the presence of indium, heat treatment of Cu 1 at.% Mn 3.8 at.% gallium at 750°C for 1 week in vacuo was performed. Heat treatment without the presence of indium appears to result in significantly higher gallium segregation as shown in Fig. 12. The theoretical curve in Fig. 12 holds for an 0.4 nm (2 monolayer) thick layer at the oxide side of the interface with a gallium concentration of 14.3 at.% per monolayer and a gallium concentration in the matrix of 2.0 at.%. From the fitted data in Fig. 12 it becomes apparent that the gallium segregation takes place at the oxide side of the interface and with the information obtained from HRTEM images a thickness of 2 monolayers appears to be consistent with this. The concentration of 14.3 at.% gallium may indicate that gallium and MnO are locally transformed into $GaMn_2O_4$. Thus, without the presence of indium, gallium segregates strongly at the oxide side of the interface and with indium present gallium only show weak signs of segregation. These results show unambiguously that indium segregation at the Cu-MnO interface seals the first monolayers at the oxide side of the boundary for the segregation of gallium.

The fitting procedure as depicted in Figs. 9–12 revealed that the fitting was always better assuming that the gallium was in the first 2 monolayers of the oxide whereas for indium this is not the case.

All the measurements were made using an electron probe that initially has an estimated size of 0.7 nm FWHM. Using the smaller 0.5 nm probe size the count rate is too low when an interface close to the hole in the TEM specimen is studied and an interface in a thicker region has to be found. On the other hand the beam broadening inside the specimen has to be taken into account and varies with the thickness to the power of 3/2. The best interfaces are found in thin areas relatively close to the hole in the specimen. A compromise has to be found between a sufficient count rate and the beam broadening. For the probe size used to generate the model curves in Figs. 9–12 a FWHM of 1.4 nm was estimated which *includes* the beam broadening in the sample. The procedure to include the beam broadening in an effective probe size is fairly accurate, although it is rather difficult to make an accurate estimate of this

effective probe size. Therefore the results of our fitting procedure, for instance the 17.6 at.% indium in the outermost monolayer of the copper matrix, suggests an accuracy that is actually not present, because due to possible variations in probe sizes the relative error is probably of the order of 30%. Consequently a more realistic value for the In concentration in the outermost layer of copper is 17.6 ± 5 at.%. Of course, there are practical solutions to know the final probe size better but at least knowledge of the drift for each data point is then necessary.

From the EDS measurement it is clear that a higher extent of segregation at heterophase interfaces results in a larger scatter among the values for the measured concentrations, especially near the maximum of the model curves. The major reason for this scatter is the drift of the sample (or electron beam) during the 40 s used to record a spectrum. The effect of drift can in principle be incorporated in the effective probe size of each individual measurement. Using the modeled curves it is assumed that the probe size is a constant for all measurement points. In practice this will not be the case and in fact the different data points correspond to curves with different effective probe sizes (see. Fig. 2(b)). Only in the case of segregation do these different effective probe sizes matter, because a straight line in the case of the absence of any segregation remains also a straight line independent of the probe size. A clear example of this is shown in Fig. 13. It holds, because segregation of Zn at the Cu-MnO interfaces does not occur. The measured Zn concentration does not show any significant scatter with respect to the straight line. All error bars in the plots of the XEDS measurements Figs. 9–13 are related to the typical errors listed in Table 2.

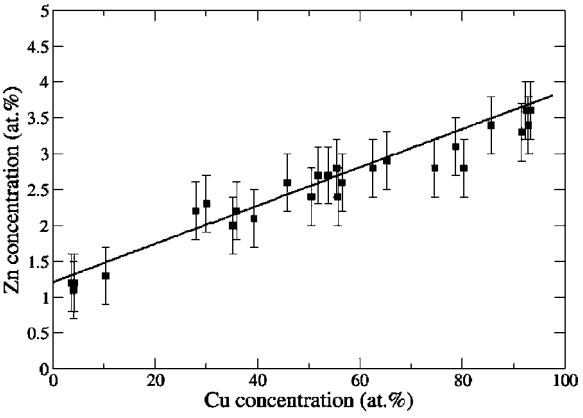

Figure 13. EDS results of Zn concentrations across a Cu-MnO interface. It indicates clearly that Zn does not segregate to the interface. However, about 1.2 at.% Zn is dissolved in the MnO precipitate. The measurement was performed with an FWHM probe size of 0.7 nm.

EDS, Selected Area Electron Diffraction patterns and HRTEM of the Ga-segregation showed that in all samples the MnO precipitates are in minority, because about 1/2 to 2/3 of the precipitates have a spinel-type structure and a composition corresponding to $Ga_xMn_yO_4$ with x varying between 1 and 2 and y between 2 and 1 (as we determined using EDS) and only the remainder is MnO. All results analyzed up to this stage hold for the MnO precipitates. An example of a spinel precipitate in copper is shown in the HRTEM image of Fig. 14. A cube-on-cube orientation relation holds between the spinel and the copper and the precipitates have octahedral shapes due to the dominant $\{111\}$ facets. The oxygen sublattices of the spinel and MnO are identical only the distribution of the cations over the interstitial sites in the O sublattice differs for the two phases. Analysis of the misfit between the copper and spinel indicates that the lattice constant of the spinel is 2 times 1.176 the lattice constant of Cu (the fcc oxygen sublattice of the spinel is measured 1.176 times larger than the fcc Cu lattice and the factor 2 arises because the unit cell of spinel is twice as big as the fcc unit cell when considering the oxygen sublattice only), i.e. using 0.3615 nm for copper this gives 0.850 nm for the spinel. This value is very close to 0.846 nm that holds for the lattice constant of the known spinel Ga_2MnO_4 (JCPDS-International 1992). The presence of $Ga_xMn_yO_4$ precipitates indicates that gallium has a tendency to react with the MnO to form a new phase. Therefore it is not completely surprising that gallium in MnO precipitates has a tendency to segregate to the oxide side of the interface. However, this is not a general rule, because for instance Zn has also a strong tendency to react with MnO to give spinel type $Zn_xMn_yO_4$ precipitates, but it does not segregate at all at Cu/MnO interfaces, neither at the oxide side nor at the metal side. A distinct difference between Zn and gallium is that the former is partially soluble in MnO, as can be seen from the 1.2 at.% Zn that is already homogeneously distributed in the MnO precipitate in Fig. 13, whereas gallium does not appear soluble in the MnO, but has to nucleate the spinel phase. Hence, the interface does not appear to form a barrier where enrichment occurs for Zn, whereas it does for Ga.

A HRTEM image of a Cu/MnO interface is shown in Fig. 15 for a sample in which gallium was dissolved (1 week 700°C) and which was annealed for

Table 2. XEDS measurements.

	Cu	Mn	O	Ga	In
Cu 1 at.% Mn 3.8 at.% Ga (just after introduction of Ga)					
Copper matrix	93.6 ± 1.2	0.5 ± 0.4	2.2 ± 1	3.8 ± 0.4	–
Cu 1 at.% Mn 3.8 at.% Ga 3.4 at.% In (after introduction of In at 750°C for 1 week)					
Copper bulk	91.8 ± 1.3	0.4 ± 0.2	2.5 ± 1.3	2.0 ± 0.3	3.4 ± 0.4
MnO precipitate	5.7 ± 1.2	51.6 ± 7.6	42.2 ± 7.1	0.2 ± 0.1	0.2 ± 0.2
Cu 1 at.% Mn 3.8 at.% Ga (after annealing at 750°C for 1 week)					
Copper matrix	92.4 ± 1.7	0.7 ± 0.5	5.1 ± 1.7	1.9 ± 0.3	–

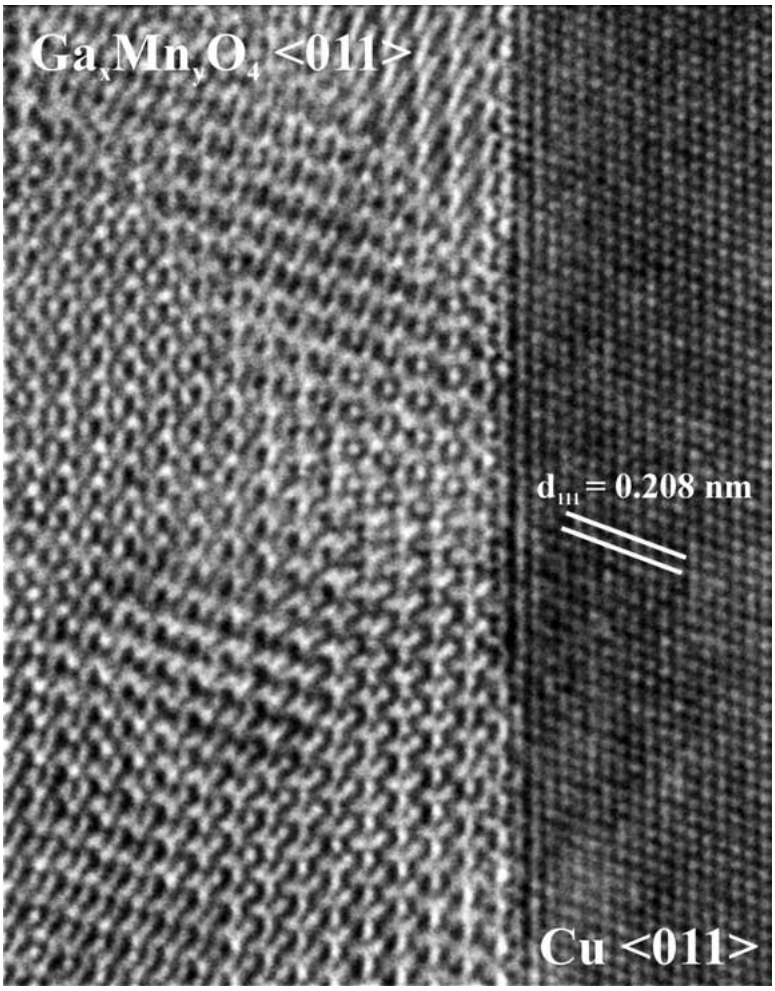

Figure 14. HRTEM image of parallel $\{111\}$ interface between Cu and the spinel $Ga_xMn_yO_4$ (where x could vary between 1 and 2 and y between 2 and 1) as viewed along a common $\langle 011 \rangle$ of Cu and spinel. In the sample Ga was dissolved by annealing for one week at 700°C during which the Ga reacted with the MnO and formed the spinel. Finally, about 1/2 to 2/3 of all precipitates became spinel and the rest remained MnO.

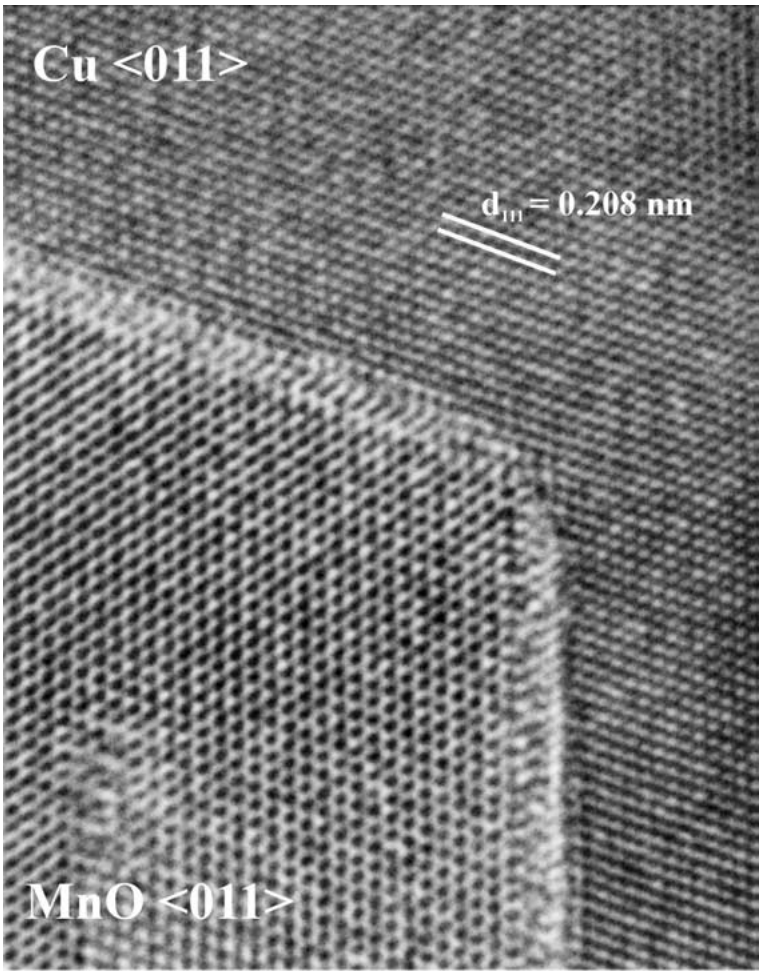

Figure 15. HRTEM image of parallel {111} Cu-MnO interfaces as viewed along a common ⟨011⟩ of Cu and MnO. In the sample Ga was dissolved by annealing for one week at 700°C and subsequently the sample was vacuum annealed for one week at 750°C. In-between the Cu and MnO a thin layer of $Ga_xMn_yO_4$ appears to be present with a thickness of about 0.5 nm that reduces the misfit at the Cu/MnO interface.

an additional week in vacuo at 750°C. The Cu-MnO interfaces are constituted by {111} planes and viewed along their common ⟨011⟩ direction. A thin layer, appearing less well ordered than the MnO and copper and positioned in-between the MnO and the copper is clearly visible in Fig. 15. The thickness of the layer is approximately 0.5 nm. The EDS measurements revealed for this case a high gallium concentration at the oxide side of the interface. Although not clearly visible, the HRTEM image indicates, based on mismatch between the thin layer and either the MnO or the Cu, that the thin layer is more intimately connected to the oxide than to the metal part. Based on mismatch it forms an intermediate between the MnO and Cu, which have a large misfit of 22.9%. The misfit of the intermediate layer is smaller with the MnO than with the Cu. Probably the phase in this intermediate layer is related to the above mentioned spinel precipitates and the spinel-type Ga_2MnO_4 (JCPDS-International 1992). The lattice constant of this spinel is 0.846 nm, compared to 0.4444 nm for MnO and 0.3615 for Cu. So, the misfit at the metal/oxide interface is reduced from 22.9% for Cu/MnO to 17.0% for Cu/spinel, where we consider the fcc oxygen sublattice with half the lattice constant of the spinel. However, based on the chemical composition (14.3 at.% Ga) it is more likely that the layer contains $GaMn_2O_4$ instead of Ga_2MnO_4. It is interesting to note that the results displayed in Fig. 15 appear quite similar to the results found for Ca segregation (enrichment) to the interface between alumina and Al [22, 23].

A plausible explanation for the gallium segregation at the oxide side of the Cu/MnO interface is that a thin outer $Ga_xMn_yO_4$ layer around the MnO reduces the metal/oxide interfacial energy by reducing the mismatch energy at the interface. In principle one sharp Cu/MnO interface is replaced by two interfaces with a thin gradient layer in-between. From a thermodynamic point of view it is probably favorable to get rid of the spinel/MnO interface and to transform the MnO fully into $Ga_xMn_yO_4$. However, in the system the total amount of Mn and O atoms is in principle fixed (in the evacuated quartz tube) and only gallium is supplied. Therefore the limiting factor for transformation of MnO into $Ga_xMn_yO_4$ is the amount of oxygen. Under this limiting oxygen condition it is impossible to transform the MnO fully, but still it appears possible to form a thin layer of $Ga_xMn_yO_4$ at the interface that apparently can reduce the interfacial energy.

The explanation for the indium segregation is straightforward. As aforementioned Indium atoms that segregate at the metal side of the Cu/MnO interface prefer the sites in-between the misfit dislocation cores of the network at the interface, because these sites offer more space for the relatively large indium atoms than present in the copper matrix. An explanation for the blocking effect of indium on the segregation of gallium to the oxide side of the interface is not as straightforward. There can be a kinetic reason: indium atoms are strongly fixed to the special sites at the interface that are also needed for the transport of gallium atoms from the copper matrix to the oxide precipitate or vice versa. In this way the gallium diffusion across the interface can be strongly hampered. However, there can also be a thermodynamic reason. It has to be kept in mind that annealing the Cu/MnO system in vacuo with gallium or indium vapor reduces strongly the oxygen partial pressure the system is subjected to. After internal oxidation the system had a tendency to become in equilibrium with the oxygen partial pressure corresponding to the dissociation pressure of Cu_2O. However, after annealing in gallium or indium vapor the oxygen partial pressure is reduced to the dissociation pressure pertaining to Ga- or In-oxide. After internal oxidation the terminating layer of MnO at the parallel $\{111\}$ Cu/MnO interface will be a close packed oxygen plane, whereas after annealing in gallium or indium vapor the terminating layer of MnO will likely become a close packed Mn plane [24, 25]. Gallium segregation at the oxide side of the interface thus implies that the terminating close packed plane of the oxide will contain a large number of gallium atoms next to the Mn atoms. Indium segregation at the metal side of the interface thus would imply a large number of In—Ga bonds across the interface. If these bonds are not favorable, as appears the case considering the binary Ga—In phase diagram [26], then the presence of indium can destabilize the presence of gallium atoms at the oxide side of the interface. On the other hand Cu—Ga bonds across the interface can be favorable (gallium is soluble in Cu, even at low temperature and can form several intermetallic phases with copper [26]). This can explain the observed results that, without the presence of indium, gallium segregates at the oxide side of the interface and, with the presence of indium, gallium segregation is hampered.

4.3. Measurement Method

The power of the present method for the measurements of segregation along hetero-interfaces relies on the fact that the *a-priori* known abrupt composition change at the interface is explicitly used. This makes the present approach in one or more ways a better choice for hetero-interface analysis than *other* techniques that are also applicable to homo-interfaces.

First of all a dedicated STEM or a STEM attachment to a (FEG-)TEM is not needed for our method although its use can improve it. A second more fundamental point is related to the accurate position of the electron probe with respect to the interface, for instance characterized by the value of A/V, with V is the volume analyzed (affected by the initial probe size and the beam broadening in the sample) and A the interface area contained in the interaction volume. For quantification of an interface segregant knowledge of the ratio A/V is important [27–29]. Positioning a nano-spot during a measurement on an edge-on oriented interface, one is never sure that the probe is *exactly* on top of the interface, i.e. with equal analyzed volumes on both sides of the interface. Still in Eqs. (6)–(9) of [27] this assumption is (without real debate) made and when applied will mostly lead to erroneous results. For instance, a misalignment of a Gaussian spot with half the distance of the FWHM of the probe, i.e of the order of Ångstroms for a nano-probe, will already decrease A/V by a factor 2. So, in practice A/V will vary between zero and the maximum attainable value according to for instance Eq. (9) in 27 (which includes beam broadening in the sample) and will *not* be simply the value in Eq. (9). These unknown variable values for A/V hold as well for line scans as for X-Ray mapping

as for energy-filtered imaging and thus will hinder an adequate quantification of the interface segregant in all these cases. A way out of this problem is to use a scan raster. With sufficient width w of the raster perpendicular to the interface plane, the value for A/V will be very robust against variations in the exact position of the raster and thus also against drift. If beam broadening is negligible, $A/V = 1/w$, where of course beam broadening is much less a problem for a scan raster than for a spot measurement with a nano-probe. A further advantage of a scan raster is the reduction of radiation damage. However, replacing a spot analysis by a raster decreases the sensitivity for detecting the segregant and also any knowledge of the distribution of the segregant in the rastered volume is lost. Still, for quantitative analysis of grain-boundary segregation the scan raster is likely to be the best choice. In contrast, for hetero-interfaces the decrease in detection sensitivity is not necessary, because the methodology presented here offers another way out of the problem with unknown variable values for A/V. In our methodology the accurate position of the probe with respect to the interface is automatically introduced after the measurements by plotting the concentration of the (segregating) solute versus one of the solvents that shows an abrupt change in concentration at the interface. This possibility to determine the exact position of the probe with respect to the interface after the measurement is only possible for hetero-interfaces presently discussed. Although there is no need to compute the values for A/V in the present approach, their variable value is intrinsic to possible obtainable results as depicted in Figs. 2, 3 and 5. For instance, Fig. 16 shows which values for A/V as a function of the Cu concentration were in fact underlying the modeled curve in Fig. 5 that fitted the experimentally obtained results.

The model has of course also limitations. One of the most important constraints is that it can be used only in systems, in which abrupt and sufficient large differences in solute concentrations A or C occur at the interface. However, for hetero-interfaces this assumption will often hold. The model assumes the electron probe to be Gaussian. This is only true if the beam generating system is working perfectly. When the model is used to determine the amount of segregation, it is assumed that the user has information about the beam diameter. This diameter however, is in the present approach heavily relying on the thickness and density of the specimen under investigation. The thickness of the TEM foil is not explicitly used but the effect of beam broadening

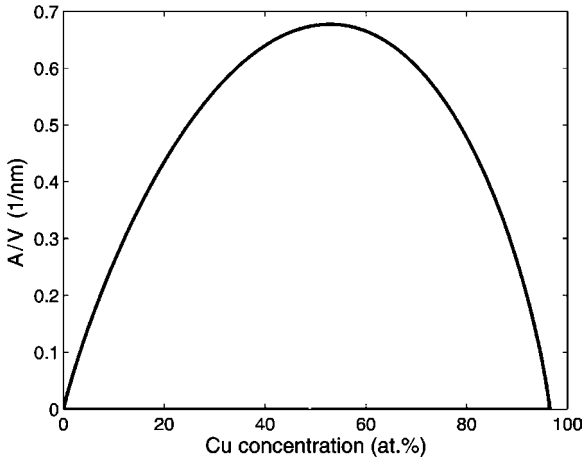

Figure 16. Values for A/V with V the analyzed volume and A the interface area in the interaction volume as a function of the Cu concentration for the modeled curve that was used to fit the experimental data in Fig. 5.

is incorporated in an increased probe size that is used for convolution. A more accurate incorporation of the beam broadening effect is possible by convoluting the concentration profiles at each thin slice dz at depth z in the TEM foil with the actual probe diameter at this depth z and then integrating over the total foil thickness. Moreover, the beam broadening is not the same on both sides of the hetero-interface. An electron beam spreads less in areas where the average atomic number and the density are lower. The final assumption that is questionable is the restriction that the enrichment is only present in a single ML. As shown at the end of Section 2 this restriction actually does not exist, but in general the experimental accuracy does not allow discrimination between segregation within a single or a double layer at the interface (cf. Fig. 3). In case of Gibbsian segregation it is often assumed that the enrichment occurs in a single ML at the interface. For instance the well-known McLean isotherms rely explicitly on this assumption. Using a line-scan or mapping it has to be verified that the type of segregation is indeed Gibbsian and does not correspond to an excess-solute profile near the interface that extends over a relative large distance away from the interface (e.g. non-equilibrium segregation).

The success of the measurement method is greatly improved if the interface is positioned accurately edge-on. In case the interface is well defined from a crystallographic point of view and planar over sufficiently large length (i.e. absence of steps and ledges) as the above parallel $\{111\}$ Cu/MnO interface it is not so difficult to

orient the interface accurately using Kikuchi-lines. Deviations of the edge-on orientation can in principle be included in the concentration profiles assumed. Instead of an atomically sharp abrupt concentration change at the interface a more gradual concentration profile can be assumed. However, generally there is not sufficient knowledge with respect to the exact experimental conditions to allow such precise assumptions. In the cases that the edge-on orientation cannot be obtained reliably the use of a scan raster should be preferred instead of the approach presented here.

The accuracy of the Analytical TEM quantification procedure is to a first approximation identical for the ML as for a general measurement of the concentrations in the bulk. For instance, for XEDS the absolute accuracy for the B/A concentration ratio will mainly rely on the accuracy of the k_{AB} factor used and for PEELS will mainly rely on the accuracy of the $\sigma_A(\Delta, \beta)/\sigma_B(\Delta, \beta)$ cross-section ratio. Due to the relative nature of the present method, it still works properly if the absolute accuracy of the concentration determination is poor (e.g. systematic errors in e.g. k_{AB}) as long as the relative accuracy of the different measurements is sufficiently high (e.g. proper counting statistics, background subtraction and integration procedure). In this case only the relative as opposed to the absolute segregation levels can be determined accurately.

In fact, in a STEM or with the use of a STEM attachment our approach can best be combined with a mapping or a scan raster technique. From a map a cell with small width w perpendicular to the interface plane is cut, just sufficient to contain pixels on both sides of the hetero-interface that are representative for the bulk phases on the two sides. The concentrations of the segregating solute obtained for the pixels in the cell are plotted against the concentration of one of the solvents obtained for the corresponding pixels. Next, the experimentally obtained results in such a plot are as before fitted with the modeled curves. Finally, the results of a scan raster can also be reproduced by averaging for each element the concentrations over all pixels in the cell with width w. This allows a comparison between the quantitative results obtained with a scan raster and the results of the fitted segregation model as proposed here.

5. Conclusions

An alternative method to measure Gibbsian segregation at heterophase interfaces using analytical TEM is proposed that offers some distinct advantages over other approaches that are also applicable to grain boundaries. The method allows quantification of the concentrations in an effective monolayer (ML) at the interface and the results are less sensitive to drift of the sample or the electron probe during the measurements and more reliable for quantification than the results of a line-scan or mapping if the latter is not combined with the present approach for solving the convolution problem. The present approach shows an improved detection sensitivity when compared with the use of a scan raster, because with a raster the measured concentration of the segregant present in for instance a monolayer at the interface decreases since is averaged over a larger volume. The requirement for the method is that at the A(B)/C(B) interface the solvents A or C show an abrupt and relative large change in concentration at the interface to which solute B may segregate. The experimentally obtained concentration of solute B is plotted as a function of solvent A (or C) and compared with simulated results having input parameters such as concentration of B in solvent A and C and in the ML at the interface and the full-width-half-maximum of the electron probe. The method is applied to the possible segregation of indium to parallel $\{111\}$ Cu/MnO interfaces. The indium concentration in the Cu matrix is 3.8 ± 0.4 at.% on average and In (and Cu) atoms do not dissolve in the MnO precipitate. The results clearly demonstrate the occurrence of segregation. A concentration of 15 ± 3 at.% In was obtained for the terminating Cu $\{111\}$ layer at the interface. On the basis of a comparison between experimental HRTEM images of the interface, atomistic calculations and image simulations it is concluded that indium atoms in this layer segregate to generalized O nodes present in-between the dislocation lines of a trigonal misfit-dislocation network with $\langle 110 \rangle$ line direction and $1/6\langle 112 \rangle$ Burgers vectors. The In atoms at the interface cause additional compressive stresses on the misfit dislocation cores present on the metal side of the interface. On theoretical grounds a favourable indium concentration at the interface of 14 ± 7 at.% is estimated which compares well with the experimental findings.

Segregation of gallium and indium and their competitive behavior at parallel $\{111\}$ Cu/MnO interfaces was analyzed using different sets of samples. In the first set that was obtained after dissolving about 3.8 at.% Ga in the copper matrix (1 week at 700°C) no significant segregation of gallium at the interfaces with the MnO

precipitates was observed. In the second set produced after additionally dissolving about 3.4 at.% indium in the copper matrix (an additional week at 750°C), weak segregation of gallium at the oxide side of the Cu-MnO interface was detected and relatively strong segregation of indium at the metal side of the interface was observed (17.6 at.% for the terminating monolayer of the copper matrix). In the third set that was obtained after annealing of the first set in vacuo for an additional week at 750°C (i.e the same treatment as for introducing In), strong segregation of gallium at the oxide side of the Cu-MnO interface was observed (about 14.3 at.% per monolayer for the first two monolayers of the oxide versus 2 at.% in the copper matrix). This leads to the conclusion that indium effectively blocks gallium segregation towards the oxide side of the interface. On the other hand, the presence of gallium does not influence the segregation of indium. Explanation for the gallium segregation at the oxide side is that a thin spinel type $Ga_xMn_yO_4$ is formed that reduces the misfit at the metal-oxide interface. Full transformation of MnO precipitates into $Ga_xMn_yO_4$ is impossible because of the limited amount of oxygen present in the system.

Acknowledgments

The Netherlands Institute for Metals Research and the Foundation for Fundamental Research on Matter (FOM-Utrecht) are acknowledged for their financial support.

References

1. W.C. Johnson and J.M. Blakely, *Interfacial Segregation* (American Society for Metals, 1977).
2. D.A. Shashkov, Atomic Scale Studies of the Structure and Chemistry of Ceramic/Metal Heterophase Interfaces, Ph.D. Thesis Northwestern University (1997).
3. P. Hayes and P. Grieveson, Met. Sci. **9**, 332 (1995).
4. D.A. Shashkov, D.A. Muller, and D.N. Seidman, Acta. Mater. **47**, 3953 (1999); J.T. Sebastian, J. Rüsing, O.C. Hellman, D.N. Seidman, W. Vriesendorp, B.J. Kooi, and J.Th.M. De Hosson, Ultramicroscopy **89**, 203 (2001).
5. M. Rühle, in *Handbook of Microscopy; Applications*, edited by S. Amelinckx, D. van Dyck, J. van Landuyt, and G. van Tendeloo (VCH, Weinheim, Germany, 1997), p. 285.
6. E. Pipel, J. Woltersdorf, J. Gegner, and R. Kirchheim, Acta Mater. **48**, 2571 (2000).
7. W. Vriesendorp, B.J. Kooi, and J.Th.M. De Hosson, Scripta Mater. **45**, 169 (2001).
8. J.R. Michael, D.B. Williams, C.F. Klein, and R. Ayer, J. Microsc. **160**, 41 (1990).
9. U. Alber, H. Müllejans, and M. Rühle, Acta Mater. **47**, 4047 (1999).
10. S.A. Dregia and P. Wynblatt, Acta Metall. Mater. **39**, 771 (1991).
11. M. Guttman and D. McLean, in *Interfacial Segregation*, edited by W.C. Johnson and J.M. Blakely (American Soc. Metals, Metals Park, Ohio, USA, 1997), p. 261.
12. F.N. Rhines and A.H. Grobe, Trans. AIME **147**, 318 (1942).
13. B.J. Kooi, H.B. Groen, and J.Th.M. De Hosson, Acta Mater. **46**, 111 (1998).
14. J.Th.M. De Hosson, H.B. Groen, B.J. Kooi, and V. Vitek, Acta Mater. **47**, 4077 (1999).
15. H.B. Groen, B.J. Kooi, W.P. Vellinga, and J.Th.M. De Hosson, Philos. Mag. A. **79**, 2083 (1999).
16. G. Cliff and G.W. Lorimer, J. Microsc. **103**, 203 (1975).
17. EDAX Phoenix software, TEM Quant Materials, version 3.2, EDAX Inc. (Mahwah, NJ, USA, 2000).
18. B.J. Kooi, O. Wouters, and J.Th.M. De Hosson, Acta Mater. **50**, 223 (2002).
19. S.J.B. Reed, Ultramicroscopy **7**, 405 (1982).
20. J.Th.M. De Hosson and B.J. Kooi, in *Handbook of Surfaces and Interfaces in Materials*, edited by H.S. Nalwa (Academic Press, 2001), Vol. 1, Ch. 1, p. 1.
21. W. Bollmann, *Crystal Defects and Crystalline Interfaces* (Springer, New York, 1970).
22. W.D. Kaplan, H. Müllejans, M. Rühle, J. Rödel, and N. Claussen, J. Am. Ceram. Soc. **78**, 2841 (1995).
23. W.D. Kaplan, Acta Mater. **46**, 2369 (1998).
24. W. Mader, Z. Metallkd. **83**, 7 (1992).
25. M. Backhaus-Ricoult and S. Laurent, Mat. Sci. Forum **294–296**, 173 (1999); M. Backhaus-Ricoult, Acta Mater. **48**, 4365 (2000); M. Backhaus-Ricoult, Acta Mater. **49**, 1747 (2000).
26. H. Baker, *ASM Handbook, Alloy Phase Diagrams* (ASM International, Materials Park, Ohio, USA, 1992), Vol. 3.
27. V.J. Keast and D.B. Williams, J. Microsc. **199**, 45 (2000).
28. J.S. Ikeda, Y.M. Chiang, A.J. Garratt-Reed, and J.B. Vander Sande, J. Amer. Ceram. Soc. **76**, 2447 (1993).
29. U. Alber, H. Müllejans, and M. Rühle, Ultramicroscopy **69**, 105 (1997).